Geophysical Prospecting

EAGE EUROPEAN ASSOCIATION OF GEOSCIENTISTS & ENGINEERS

Geophysical Prospecting, 2010, **58**, 361–373 doi: 10.1111/j.1365-2478.2009.00828.x

Seismic interferometry, intrinsic losses and *Q*-estimation*

Deyan Draganov†, Ranajit Ghose, Elmer Ruigrok, Jan Thorbecke and Kees Wapenaar

Department of Geotechnology, Delft University of Technology, PO Box 5048, 2600 GA Delft, the Netherlands

Received December 2008, revision accepted July 2009

ABSTRACT

Seismic interferometry is the process of generating new seismic traces from the cross-correlation, convolution or deconvolution of existing traces. One of the starting assumptions for deriving the representations for seismic interferometry by cross-correlation is that there is no intrinsic loss in the medium where the recordings are performed. In practice, this condition is not always met. Here, we investigate the effect of intrinsic losses in the medium on the results retrieved from seismic interferometry by cross-correlation. First, we show results from a laboratory experiment in a homogeneous sand chamber with strong losses. Then, using numerical modelling results, we show that in the case of a lossy medium ghost reflections will appear in the cross-correlation result when internal multiple scattering occurs. We also show that if a loss compensation is applied to the traces to be correlated, these ghosts in the retrieved result can be weakened, can disappear, or can reverse their polarity. This compensation process can be used to estimate the quality factor in the medium.

INTRODUCTION

In its most general definition, seismic interferometry is the process of generating new seismic responses from the cross-correlation, convolution, or deconvolution of existing traces. Claerbout (1968) proposed to retrieve the reflection response of a 1D medium from the autocorrelation of the transmission response. Later, he conjectured that for a 3D medium, the reflection response could be retrieved from cross-correlation of observed seismic noise (Rickett and Claerbout 1996). Since the beginning of this century, different researchers have shown how one can extract the seismic impulse response (the Green's function) from the cross-correlation of observations from transient or noise sources (e.g., see Schuster 2001; Campillo and Paul 2003; Shapiro and Campillo 2004). For an extensive overview, the reader is referred to Schuster (2009) and Wapenaar, Draganov and Robertsson (2008a). Lately, the theory has been extended to electromagnetic and electroseismic observations (Wapenaar, Slob and Snieder 2006; Slob, Draganov and Wapenaar 2007; Wapenaar *et al.* 2006).

One of the main assumptions in seismic interferometry by cross-correlation is that there are no intrinsic losses in the medium where the recordings are made. Starting with this assumption and consequently making use of the principle of time-reversal invariance of the wave equation, it is shown that, taking the acoustic case as an example, the Green's function $G(\mathbf{x}_A, \mathbf{x}_B, t)$ and its time-reversed version, that would be measured at a receiver at point $\mathbf{x}_A$ due to an impulsive source at $\mathbf{x}_B$, can be obtained from the relation (Wapenaar and Fokkema 2006):

$$G(\mathbf{x}_A, \mathbf{x}_B, t) + G(\mathbf{x}_A, \mathbf{x}_B, -t) \approx \frac{2}{\rho c} \oint_{\partial \mathbb{D}} G(\mathbf{x}_B, \mathbf{x}, t) * G(\mathbf{x}_A, \mathbf{x}, -t)\, d^2\mathbf{x}. \quad (1)$$

In the above relation, c and ρ are the constant propagation velocity and mass density, respectively, at and outside surface $\partial\mathbb{D}$ that effectively surrounds $\mathbf{x}_A$ and $\mathbf{x}_B$ and $*$ denotes

*This paper is based on the extended abstract G024 presented at the 70th EAGE Conference & Exhibition Incorporating SPE EUROPEC 2008, 9–12 June 2008 in Rome, Italy.

†E-mail: d.s.draganov@tudelft.nl

convolution. In the right-hand side of the above equation one cross-correlates recordings at the points $\mathbf{x}_{\mathcal{A}}$ and $\mathbf{x}_{\mathcal{B}}$, when these recordings result from sources at positions $\mathbf{x}$ on the surface $\partial\mathbb{D}$. Relation (1) is obtained from an exact equation as the latter is not very useful for practical applications. The exact equation contains in its right-hand side two integrals of cross-correlations of responses from monopole and dipole sources. To transform it to the more practical relation (1) with one integral of cross-correlations of responses from monopole sources only, it has been assumed that the dominant wavelengths of the fields are small compared to the size of the inhomogeneities (high-frequency approximation) and that $\partial\mathbb{D}$ is a sphere with a very large radius (far-field approximation). These approximations result in mainly amplitude errors.

When there are intrinsic losses in the medium of interest, Snieder (2006, 2007) showed that equation (1) should be extended to include at the two observation points cross-correlations from sources inside the complete volume $\mathbb{D}$ enclosed by the boundary $\partial\mathbb{D}$:

$$G(\mathbf{x}_{\mathcal{A}}, \mathbf{x}_{\mathcal{B}}, t) + G(\mathbf{x}_{\mathcal{A}}, \mathbf{x}_{\mathcal{B}}, -t) \approx \frac{2}{\rho c}\oint_{\partial\mathbb{D}} G(\mathbf{x}_{\mathcal{B}}, \mathbf{x}, t) * G(\mathbf{x}_{\mathcal{A}}, \mathbf{x}, -t)\, d^2\mathbf{x} + \int_{\mathbb{D}} (b^p(\mathbf{x}, t) + b^p(\mathbf{x}, -t)) * G(\mathbf{x}_{\mathcal{B}}, \mathbf{x}, t) * G(\mathbf{x}_{\mathcal{A}}, \mathbf{x}, -t)\, d^3\mathbf{x}, \tag{2}$$

where, following the notation of Wapenaar *et al.* (2006), $b^p(\mathbf{x})$ is the medium's loss factor related to the compressibility. The loss factor related to the mass density has been assumed to be zero. In practical applications for laboratory or field experiments, the condition of a lossless medium will not always be met. This means that to apply seismic interferometry, one would need to resort to equation (2). However, in general it will be very difficult to find a situation where there would be a distribution of sources inside the complete volume of interest. The situation would become even more complicated, if the loss factor related to the mass density is not zero. In this case, a second volume integral would appear on the right-hand side of equation (2) with cross-correlation at the two observation points of recordings from dipole sources in $\mathbb{D}$, whereas in equation (2) the volume integration is only over recordings from monopole sources.

It is most likely that in real situations the sources in the media will only be confined to some small part (or several parts) of the volume, which means that one should look for alternatives to equation (2). One alternative, which accounts for intrinsic losses, was introduced by Slob *et al.* (2007) (see also Halliday and Curtis (2009) for an application to scattered surface waves). They proposed to use seismic interferometry by convolution, where one of the observation points should be outside the boundary $\partial\mathbb{D}$, while the other observation point should still lie inside $\partial\mathbb{D}$. Even though this method needs only a surface integral over the sources, it is not always a practical solution as in most seismic applications both receivers will be inside $\partial\mathbb{D}$. Recently, Wapenaar, Slob and Snieder (2008b) proposed an alternative that accounts for intrinsic losses – seismic interferometry by multidimensional deconvolution. One extra advantage of seismic interferometry by multidimensional deconvolution is that it can compensate for irregular source distribution and different source strengths. An additional requirement of the deconvolution method is that a matrix inversion is made of simultaneous recordings at many receivers to obtain the Green's function between the two points of interest. Contrary to this, seismic interferometry by cross-correlation can be performed with recordings only at the two points of interest. Vasconcelos and Snieder (2008a,b) proposed to use trace deconvolution before summation over the sources on $\partial\mathbb{D}$. This method does not require matrix inversion of simultaneous recordings but intrinsically assumes a 1D medium.

For the above reasons, it will still be desirable to make use of relation (1) in a lot of practical applications. In the following, we investigate what are the effects of intrinsic losses on the results from seismic interferometry by cross-correlation. We start our investigation using the simplest case – a homogeneous model, and slowly increase the degree of difficulty by using a layered model and finally a general inhomogeneous model with internal scattering. Slob *et al.* (2007) used numerical modelling results for electromagnetic waves in a two-layer medium with intrinsic losses to test the electromagnetic variant of equation (1). They showed that the cross-correlation method would still retrieve the Green's function but that later arrivals might not be retrieved. In section 'Laboratory results for a homogeneous sand chamber' we test this finding on a scalar-wavefield laboratory dataset for a homogeneous medium. Tanter, Thomas and Fink (1998) showed that to improve the result of the application of time-reversal acoustics (a method related to seismic interferometry by cross-correlation) for focusing in the brain through the scull, i.e, in the presence of losses, a loss compensation should be applied before time reversal. In section 'Modelling results for inhomogeneous media', we will work out a similar approach for seismic interferometry and will further show how our approach can be used to estimate the effective quality factor (Q) of the overburden.

LABORATORY RESULTS FOR A HOMOGENEOUS SAND CHAMBER

We start our investigation of the effect of intrinsic losses on the results from SI by cross-correlation using a homogeneous physical model. The goal was to directly check the effect of a varying damping, introduced by varying the source frequency, on the reflection response retrieved by cross-correlation. The data for this experiment were acquired in a water-tight cylindrical chamber filled with unconsolidated sand, see Fig. 1. Special attention was paid to keep the sand in a loose, unconsolidated condition, because unconsolidated sand, with low Q, causes strong attenuation of the propagating seismic-wave energy (e.g., see Musset and Khan 2000; Priest, Best and Clayton 2005). The sand sample was prepared through pluviation of sand in water making the sample quite homogeneous. The chamber consisted of 34 plastic (PVC) rings standing on a steel base. Piezoelectric bender elements served as source and receiver. The source and the receiver were positioned in the middle points at the top and bottom of the sample, respectively. The measurements were performed following the idea of a 'gradually vanishing sample'. The initial height of the sample was 501 mm. A source transducer acting as a source for S-wave polarized in the horizontal direction (SH-wave) was placed on top of the sample at location S (see Fig. 1) and was set off. The resulting waves, transmitted through the unconsolidated sand, were recorded at the receiver location R by a transducer sensitive in a direction parallel to the SH-wave polarization. After this, the top ring was carefully sliced off, the source transducer was lowered to the new height of the sample, now 486 mm and a new transmission measurement was performed (Fig. 2). This procedure was repeated

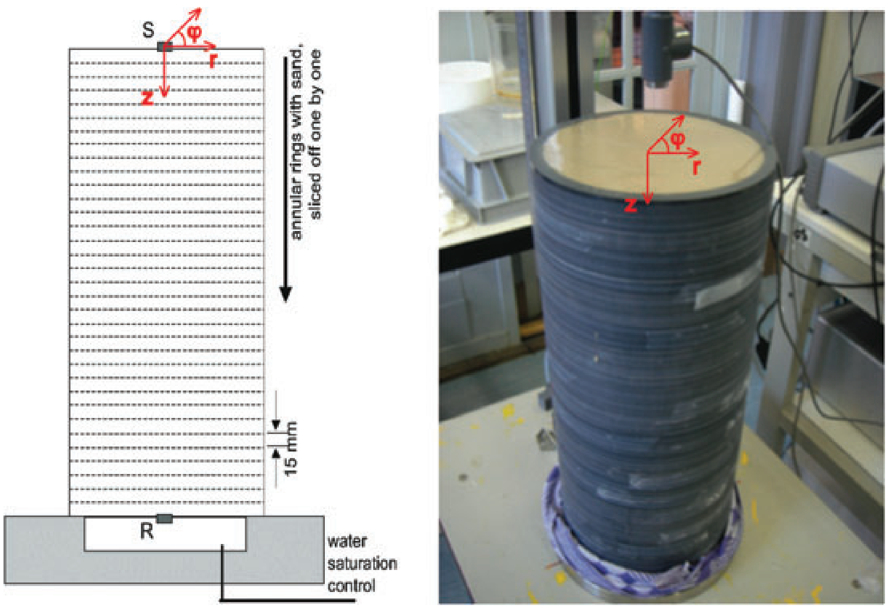

Figure 1 A homogeneous sand chamber for measuring transmission responses. S denotes a source of SH-waves and R denotes a receiver sensitive in the direction of the SH-wave motion. The red coordinate system indicates the orientation of the vertical axis z, the radius r and the azimuth ϕ. The sample consists of 34 plastic rings, each with a diameter of 225 mm and a height of 15 mm, except the lowest one, which was 6 mm high.

Figure 2 The measurements are performed using a 'vanishing' sample: after a measurement is finished, the top ring is sliced off and a new measurement is taken with the source placed at the new top.

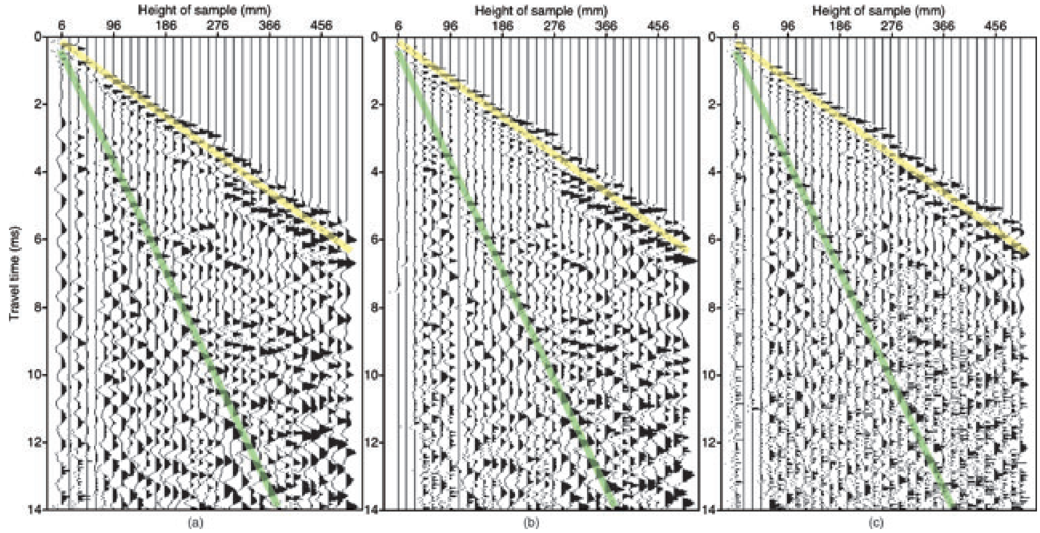

Figure 3 Observed transmission panels for the configuration in Fig. 1 for a source central frequency of **a)** 3 kHz, **b)** 6 kHz and **c)** 18 kHz. The panels are shown after application of automatic gain control to bring forward also the later arrivals. The yellow and green lines highlight the direct transmission and its multiple, respectively.

until only the last ring was left. Note that this measurement scheme allowed us to measure the waves for different heights of the sand sample and still keep the medium homogeneous for each height level. The measurements resulted in 34 traces, combined in one panel (see Fig. 3).

Because we used both an SH-wave source and an SH-wave receiver, the predominant energy in our recorded wavefield was SH and therefore, the wave propagation here was considered to obey the scalar wave equation. However, due to imperfect coupling and finite dimensions of the transducer elements and due to the mode conversions at the chamber wall, some compressional (P) wave and vertically polarized shear (SV) wave energy was also present in the data. Particularly, P-wave arrivals were visible before the arrival of the earliest SH-waves. This energy was muted before further processing. Due to the cylindrical symmetry of the chamber, the experiment could further be considered as independent of the azimuth.

For each source location three different measurements were performed by changing the central frequency of the source. The central frequencies were set to 3, 6 and 18 kHz, respectively. On the three resulting recorded panels shown in Fig. 3, we can observe the direct transmission arrival, highlighted by the yellow lines and its multiple that had bounced between the bottom and the top of the sample, highlighted by the green lines. We can also see reflections from the side walls of the chamber and their multiples. For our purposes, we concentrated on the transmissions. From the transmission measurements we estimated the quality factor of the loose sand to be around $Q = 16$. For this purpose, we used the band-limited spectral ratio of the measurements (Tonn 1991). We did this for each source central frequency and then averaged the results for the three frequency bands. Our estimated average quality factor $Q = 16$ for shear waves in unconsolidated sand is realistic (e.g., Hu and Su 1999) have reported shear-wave $Q < 10$ for soft soil deposits and $Q = 30$ for weathered bedrock at a shallow depth). In the following, we assume that the estimated average Q is the same for all three data sets corresponding to the three different source frequencies. In reality, the effective damping for the three experiments is different and increases with increasing frequency of the source wavelet. This can be seen in Fig. 3, where, due to strong attenuation of the high frequencies, the frequency content of the middle and right panels is not too much different from the one of the left panel.

We apply seismic interferometry to the observed transmissions with the aim to retrieve reflections between the top and the bottom of the chamber. We use the modified form of equation (1) for coinciding observation points, i.e.,

$$G(\mathbf{x}_R, \mathbf{x}_R, t) + G(\mathbf{x}_R, \mathbf{x}_R, -t) \approx \frac{2}{\rho c} G(\mathbf{x}_R, \mathbf{x}_S, t) * G(\mathbf{x}_R, \mathbf{x}_S, -t). \tag{3}$$

Because the source S and the receiver R lie on the cylinder's axis and due to the cylindrical symmetry of the sand sample, for the retrieval of the reflection response we can suffice with only one source at the top of the sample and thus the integral over different source positions is omitted. The results of

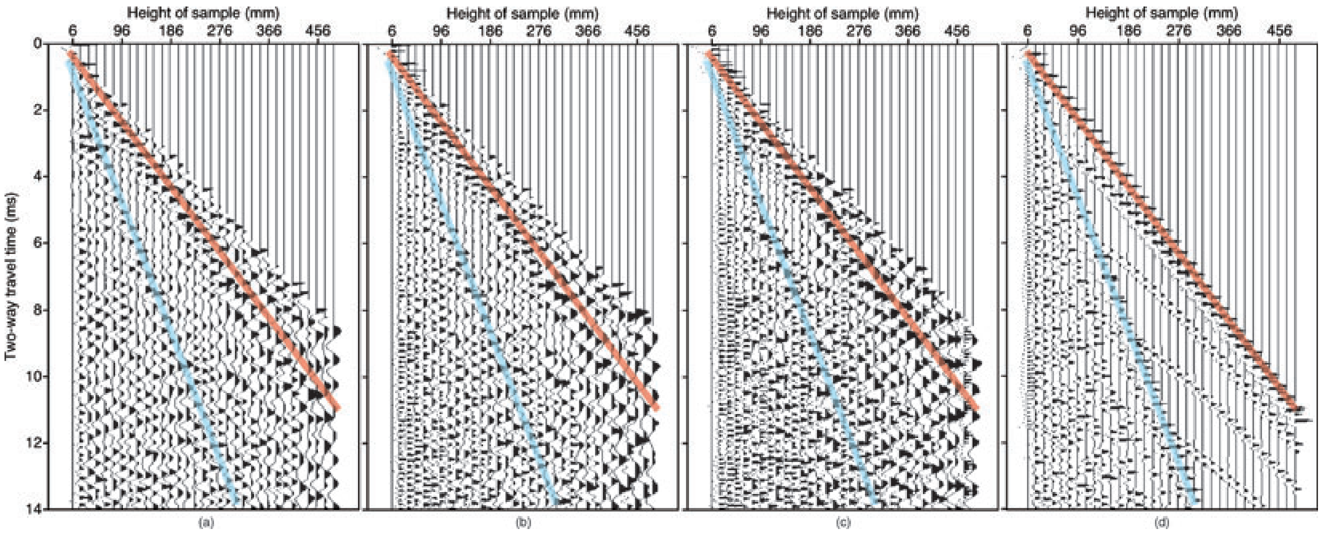

Figure 4 Reflection response of the sand chamber for coincident source and receiver positions at the bottom of the sample at R. Retrieved reflection response was obtained from the autocorrelation of the observed transmission responses for source central frequencies of **a**) 3 kHz, **b**) 6 kHz and **c**) 18 kHz. For comparison purposes, (**d**) shows a finite-difference modelled reflection response. The event highlighted in red represents the reflection from the top of the cylindrical sample. The event highlighted in blue represents the multiple reflection that has bounced twice from the top of the chamber. The panels are shown after application of automatic gain control to bring forward also the later arrivals.

the application of equation (3) to the transmission measurements for the three different source frequencies are shown in Fig. 4(a-c). Here the negative times were muted and automatic gain control was applied to bring forward the later arrivals. We refrained from filtering the noisy data sets of the laboratory experiments and highlighting the top and bottom reflected events, because we wanted to examine whether seismic interferometry works well even when the signal has suffered from strong attenuation. Each of the three panels represents the retrieved reflection response of the vanishing sample for coincident source and receiver positions at the bottom of the chamber. As no reflection measurements were performed during the laboratory experiment, to be able to evaluate the quality of the retrieved results, we compared the results with a numerically modelled reflection response. The modelling was performed using a scalar finite-difference scheme. The model represented a homogeneous medium limited from all sides by reflecting boundaries. The propagation velocity and quality factor were taken to be 90 m/s and 16, respectively, as estimated from the transmission data. We used a source central frequency of 3 kHz. The modelled reflection response is shown in Fig. 4(d). Comparing kinematically the retrieved results with the modelled data, we see that the reflection from the top of the sample (the event highlighted with red) is retrieved but the quality of the retrieved result decreases with increasing central frequency of the source wavelet. In panels (4b) and (4c), the higher frequency signals are strongly damped when the height of the sample increases. This results in a low signal-to-noise ratio and, consequently, the reflection from the top is less clear. This observation is even more conspicuous for the multiple reflection highlighted with blue, which has bounced twice off the chamber's top. In Fig. 4(a) the multiple is readily interpretable, in Fig. 4(b) it is harder to discern, while in Fig. 4(c) it is drowned in the background noise generated by the correlation process. This example confirms the conclusion of Slob *et al.* (2007) that in a dissipative medium SI by cross-correlation would retrieve the Green's function but in case of strong losses the later arrivals might not be retrieved well.

MODELLING RESULTS FOR INHOMOGENEOUS MEDIA

We saw that in the simplest case of a homogeneous medium or a medium consisting of two layers, seismic interferometry by cross-correlation relation, i.e., equation (1), can be used to retrieve the kinematics of the Green's function. In this section, we investigate a more complex situation, where the medium causes internal scattering, for example when internal multiples are generated.

Horizontally layered subsurface

It is instructive to investigate first the influence of intrinsic losses on a subsurface model, as depicted in Fig. 5(a), which

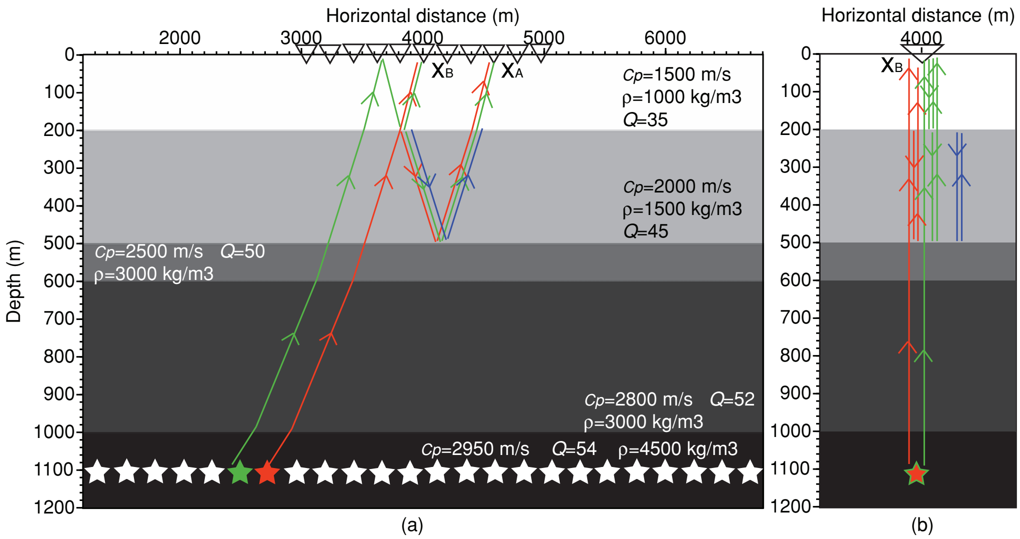

Figure 5 **a**) Acoustic subsurface model used in a finite-difference modelling scheme to generate transmission gathers from each of the subsurface sources (the stars) to the receiver array (the triangles). Each subsurface layer was characterized by its propagation velocity c_p, mass density ρ and quality factor Q. The red and green pointers suggest raypaths from the sources in the subsurface to the receivers. The blue pointers suggest a raypath from a source to a receiver on the boundary between the first and the second layer. **b**) Explanation of the appearance of ghost events for coinciding $\mathbf{x}_A$ and $\mathbf{x}_B$.

consists of five horizontal layers below a free surface. We used 201 receivers (the triangles) at the free surface between 3000–5000 m placed every 10 m. 225 subsurface sources (the stars) lay at depth level 1100 m and were evenly distributed in the horizontal direction every 25 m between 1200 m–6800 m. We looked at two situations: in the first one, the subsurface was lossless; in the second one, the subsurface was dissipative, where the dissipation was modelled only as amplitude damping. In the latter case, we took the attenuation to be linear with frequency, i.e, we described the losses by a constant Q. It is generally considered that for the frequency band used in exploration seismics, the quality factor can be taken to be constant (see, e.g., McDonal *et al.* 1958; Kjartansson 1979). The values for Q were chosen to be equal to the square root of the P-wave velocities of the layers (Mittet 2007). We used an acoustic finite-difference scheme to model transmission gathers from each of the subsurface sources to the receiver array. We applied equation (1) to the modelled data in the following way. We chose a master trace, for example the trace at $\mathbf{x}_B = (4000, 0 \text{ m})$, where, after the cross-correlation, we would obtain a virtual source. This trace was correlated with the entire common-source gather (different points $\mathbf{x}_A$) to obtain a correlated transmission gather. The correlation process was repeated for all subsurface source positions to obtain 225 correlated transmission gathers. These gathers were then resorted into correlated common-receiver gathers representing the integrand on the right-hand side of equation (1). Note that, due to the presence of the free surface, the closed boundary integral in equation (1) can be replaced by an open boundary integral along the sources in the subsurface. For the model without intrinsic losses, Fig. 6(a) depicts a correlated common-receiver gather for coinciding $\mathbf{x}_A$ and $\mathbf{x}_B$ for all subsurface source positions. The traces in a correlated common-receiver gather were then summed together to produce a final retrieved trace (Fig. 6b) for a virtual source at the position of the master trace. The retrieved events in Fig. 6(b) result from constructive interference in the stationary-phase regions (Schuster, Yu and Rickett 2004; Snieder 2004) of events in Fig. 6(a). The stationary-phase regions are indicated by the yellow rectangle. For example, the events at 0.26 s and −0.26 s are actually the retrieved zero-offset causal and acausal reflections, respectively, from the first interface in Fig. 5(a). The correlation pattern of the events in Fig. 6(a) results from the traveltime difference between waves recorded at the observation points and generated by the same source. In the stationary-phase region, the absolute value of the difference is biggest. In Fig. 6(a) it can also be observed that there are stationary-phase regions, highlighted with the blue rectangles that have weaker amplitudes. When summed, these regions will not produce a retrieved arrival in Fig. 6(b). The weaker amplitudes are a result of the mutual cancellation of two correlated events that in the stationary-phase regions arrive at the same times but with opposite polarities. This can be explained using the red and green rays depicted in

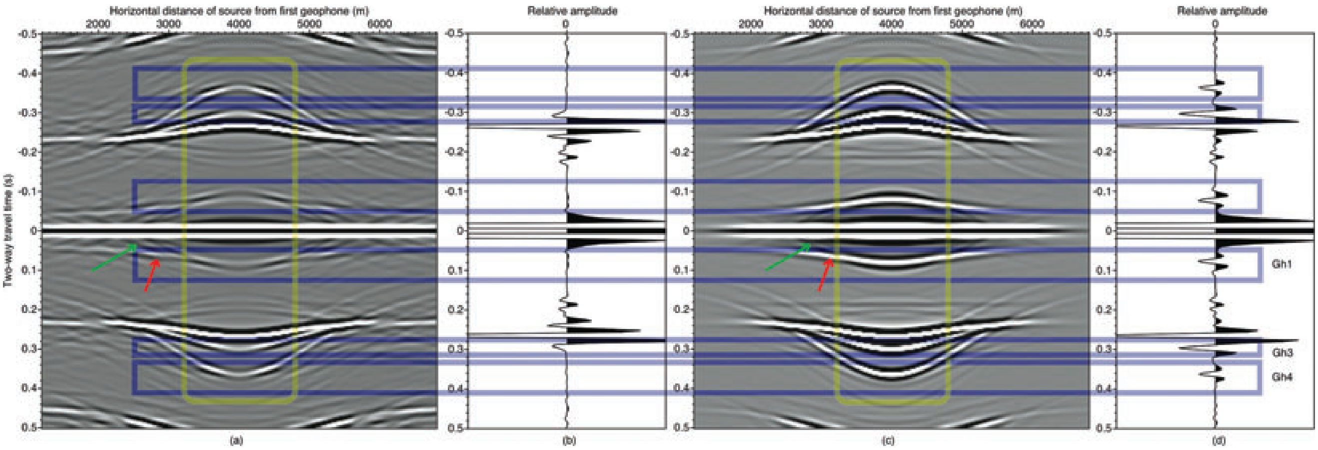

Figure 6 **a)** Common-receiver gather of the master trace at 4000 m correlated with itself for the model without intrinsic losses. **b)** The result of the summation over the source positions in (a), i.e., the retrieved zero-offset trace at 4000 m. **c)** As in (a), but for a model with intrinsic losses. **d)** As in (b), but with intrinsic losses. The yellow rectangles indicate stationary-phase regions, while the blue rectangles indicate coinciding stationary-phase regions that mutually cancel when no losses are present in the model. Gh1, Gh3, and Gh4 indicate non-physical (ghost) events that appear in the correlation result due to the intrinsic losses in the medium. The red and green pointers clarify the two correlation results that cancel each other in (a) but do not cancel each other in (c).

Fig. 5(b). The subsurface source emits a wave that is recorded as a direct arrival at the receiver following the red ray. After the direct wave, we would record a later arrival containing an internal multiple from the second layer. When these two arrivals are cross-correlated, the correlation process eliminates the common travelpaths and we are left with an event that would have propagated only along the blue ray. Following the green ray, at the receiver we record a free-surface multiple of the direct arrival followed by a free-surface multiple of the arrival containing the internal multiple from the second layer. If these two latter arrivals are correlated, the common travelpaths are eliminated and we are again left with an event that would have propagated only along the blue ray but this time the correlation result exhibits opposite polarity. If the two correlation results, which appear to have propagated only along the blue ray, are summed together, they will cancel each other. The same reasoning is valid for all sources inside the stationary-phase region. For sources outside this region, the two correlation results do not overlap, see the red and green arrows in Fig. 6(a).

We repeated the correlation procedure for obtaining the results in Fig. 6(a,b), but this time for the subsurface model with intrinsic losses. The results are shown in Fig. 6(c,d). We can see that there is no mutual cancellation anymore inside the blue rectangles in (c) and non-physical events – ghosts – appear in Fig. 6(d). Due to the intrinsic losses in the model, the recordings at the coinciding receivers $\mathbf{x}_{\mathcal{B}}$ and $\mathbf{x}_{\mathcal{A}}$ in Fig. 5(b), which we observe following the green ray, are now damped stronger compared to the recordings following the red ray. The stronger damping comes from the extra propagation of the waves along the green ray inside the first layer. This means that after cross-correlation the two events along the blue travelpath will have different amplitudes and will not cancel each other. Note that using the explanation in Fig. 5(b), the resulting ghost event will appear in the final retrieved result at a time of an internal reflection measured with a source and a receiver both lying on the boundary between the first and second layers (Ruigrok, Draganov and Wapenaar 2008).

When the observation points $\mathbf{x}_{\mathcal{B}}$ and $\mathbf{x}_{\mathcal{A}}$ do not coincide, we still observe the same effect. The difference is that the red and green rays do not overlay each other and originate from different sources. This is depicted in Fig. 5(a). Nevertheless, the red and green rays are parallel and the only difference in damping will again come from the extra propagation of waves along the green ray inside the first layer. Figure 7(a,b) shows the retrieved common-source gathers for the model without and with intrinsic losses, respectively, for a virtual source at 4000 m. Comparing the two results, we see that several ghosts, indicated with Gh1–Gh5, are easily identifiable on Fig. 7(b). Ghost Gh1 results from an internal multiple in the third layer, Gh2 from an internal multiple in the fourth layer, Gh3 from an internal multiple in the second layer, Gh4 from an internal multiple between the top of the third and the bottom of the fourth layer and Gh5 between the top of the second and the bottom of the third layer. The origin of the ghost events Gh1,

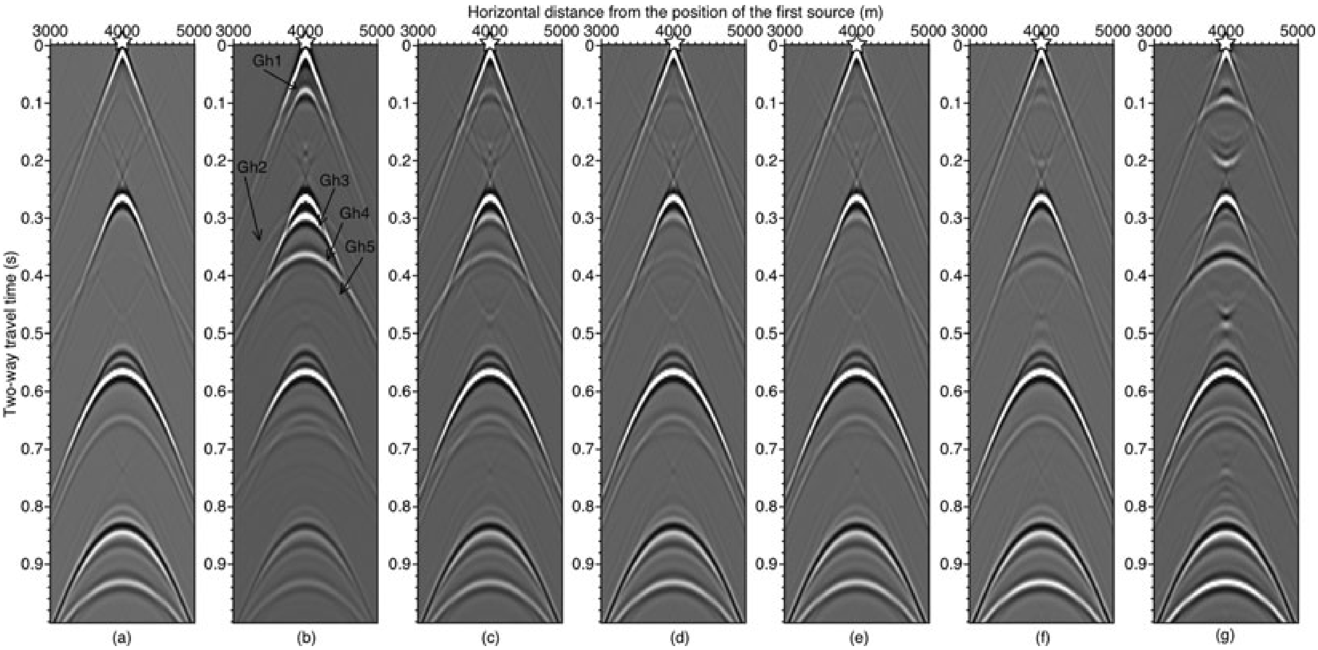

Figure 7 Retrieved reflection response of the subsurface model in Fig. 5 for a virtual source at the surface at horizontal position 4000 m. **a**) Interferometry result for a lossless medium. **b**) Interferometry result for a medium with intrinsic losses. **c**) The seismic interferometry result when the correlation is performed on transmission panels with a damping-compensation factor $Q = 50$. **d**) As in (c) but for $Q = 40.7$. **e**) As in (c) but for $Q = 39.7$. **f**) As in (c) but for $Q = 35$. **g**) As in (c) but for $Q = 30$.

Gh3 and Gh4 can be traced in Fig. 6(c,d), where they are indicated.

The finite-difference modelling scheme that we use incorporates the intrinsic loss as an amplitude damping (Aki and Richards 2002) by multiplying the wavefields with a damping factor $e^{-\frac{t\pi f_0}{Q_{layer}}}$, where f_0 is the central frequency of the source wavelet and Q_{layer} is the quality factor per layer. Based on the above explanation of the appearance of the ghosts, we propose a simple procedure for the identification of the ghost arrivals. In each modelled common-source transmission gather the damping due to the intrinsic losses is compensated for by multiplying the recordings by $e^{\frac{t\pi f_0}{Q}}$, where

$$Q = \frac{\sum_i \frac{d^i}{c_p^i}}{\sum_i \frac{d^i}{c_p^i Q^i}} \tag{4}$$

is an effective damping-compensation factor representative for the overburden with d^i, c_p^i, and Q^i the thickness, P-wave velocity and quality factor, respectively, of each of the layers that comprise the overburden. Figure 7(c-g) shows the retrieved common-source reflection gathers for a virtual source at 4000 m after applying damping compensation with $Q = 50$, $Q = 40.7$, $Q = 39.7$, $Q = 35$, and $Q = 30$. Tracing the ghost event Gh1 from Fig. 7(c-g), we see that in Figs 7(c) and 7(d) its amplitude is lowered, in Fig. 7(e) the event is nearly invisible, while in Figs 7(f) and 7(g) it appears again but with reversed polarity. A similar effect is observed for the other ghosts. For example, ghosts Gh3 and Gh5 disappear in Fig. 7(f) and reappear in Fig. 7(g) with reversed polarity; Gh2 disappears in Fig. 7(d) and after that reappears with reversed polarity. On the other hand, the real reflections always keep their polarity regardless of the applied Q-compensation. These observations dictate the procedure for the identification of the ghost events: to apply Q-compensation with several values to each of the recorded common-source gathers before cross-correlation and then look in the retrieved result which events have changed their polarity. When the ghosts are identified, they can be muted from the retrieved results. We propose to use the damping-compensation procedure also for Q-estimation. The value $Q = 39.7$, at which Gh1 disappeared, is actually the effective Q of the medium above the third layer (the layer that caused Gh1 to appear). Similarly, Gh2 disappeared at $Q = 40.7$, which is the effective Q of the overburden above the fourth layer; Gh3 disappeared at $Q = 35$, which is the Q in the first layer. This means that the Q-compensation procedure estimates the effective Q of the overburden above each ghost-producing layer. To save computational cost,

Q might be estimated using only two receivers, instead of applying the procedure to the complete receiver array. Figure 8(a-g) show the Q-estimation using the zero-offset traces from Fig. 7(a-g), respectively.

General inhomogeneous subsurface

In a more general inhomogeneous medium, the ghosts due to the intrinsic losses can be identified by applying the Q-compensation procedure in the same way as for the horizontally layered situation. The situation when one wants to apply Q-estimation requires more attention. We illustrate this using the model in Fig. 9, where the subsurface sources are not distributed at the same depth level (in this case, the sources are distributed randomly in the vertical direction between 700–850 m), which comes closer to a realistic source distribution. Because of this and because of the complex subsurface, waves that propagate along the green ray to the free surface will experience in general different damping than the waves travelling along the red ray to the free surface. This means that after cross-correlation, the two events representing propagation along the blue ray will mutually cancel only when the transmission common-source gathers would be compensated for a total quality factor Q that depends on the difference in damping of the waves following the complete paths from the sources to the free surface along the green and red rays. The only exception is the retrieved zero-offset trace. For this trace the red and green sources, respectively rays, will coincide and the estimated Q will be the effective Q of the overburden above each ghost-producing layer. We illustrate this with the retrieved results in Figs 10 and 11. Making a parallel between this subsurface model and the horizontally layered model from section ‘Horizontally layered subsurface’, we would expect also here to see five ghost events that have

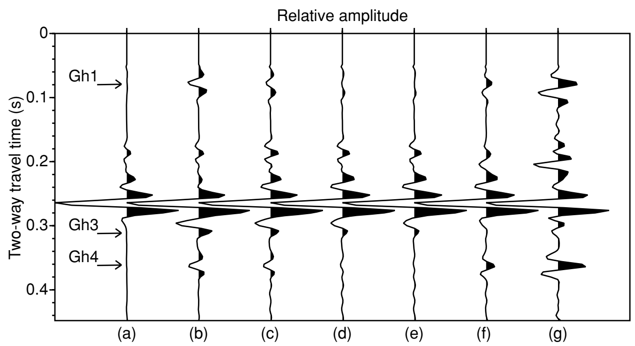

Figure 8 Retrieved zero-offset traces at horizontal position 4000 m for the subsurface model from Fig. 5, **a)** without intrinsic losses, **b)** with intrinsic losses and when damping compensation is applied with **(c)** $Q = 50$, **(d)** $Q = 40.7$, **(e)** $Q = 39.7$, **(f)** $Q = 35$, and **(g)** $Q = 30$. All traces are scaled to the maximum amplitude in each trace.

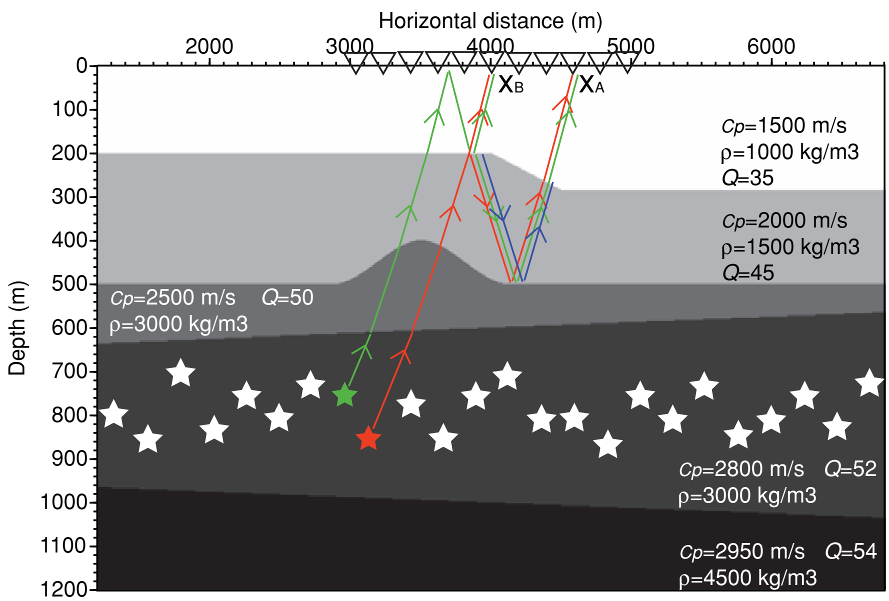

Figure 9 Acoustic subsurface model used in a finite-difference modelling scheme to generate transmission common-source gathers. The first reflective boundary from the top has an offset created by a fault, the second boundary features an anticline. The lowest two reflective boundaries represent dipping reflectors. Each subsurface layer is characterized by its propagation velocity c_p, mass density ρ and quality factor Q. The subsurface sources were distributed in the horizontal direction every 25 m from 1200–6800 m, while in the vertical direction they were randomly placed between depth levels 700–850 m.

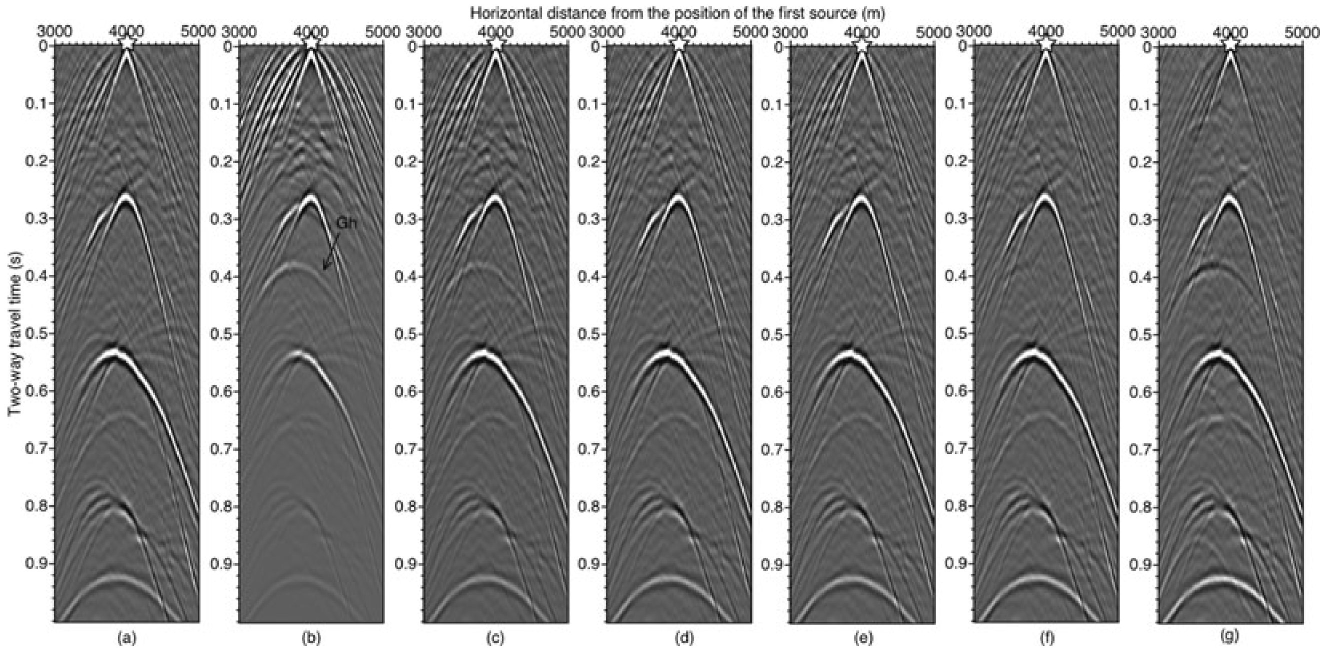

Figure 10 As in Fig. 7 but for the subsurface model from Fig. 9.

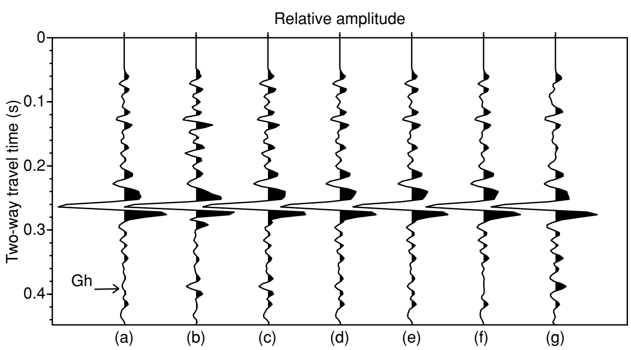

Figure 11 As in Fig. 8 but for the subsurface model from Fig. 9.

arisen due to the intrinsic losses. But due to the complexity of the subsurface model and source distribution, only one ghost, labelled Gh, is clearly visible in Fig. 10(b). This ghost was caused by an internal multiple between the top of the second layer and the bottom of the third layer. Due to illumination issues, the rest of the ghosts appear as correlation artefacts in both the retrieved results without losses (Fig. 10a) and with losses (Fig. 10b).

When we apply the Q-compensation procedure to the common-source transmission gathers and correlate them, looking at Fig. 10(c)-(g) we can easily identify the ghost. On the other hand, it is more difficult to conclude which Q caused the ghost to disappear – panels Fig. 10(d,e) both appear to produce the best results. Thus, we might conclude that the effective Q of the overburden is around 40. When we look at the zero-offset traces in Fig. 11 though and follow Gh from Fig. 11(c-g), we see that the best compensation is achieved with $Q = 35$ (Fig. 11f), which is the actual effective Q of the overburden, i.e., of the first layer.

DISCUSSION

As shown above, application of seismic interferometry by cross-correlation to the response of a dissipative medium with internal multiples will result in the appearance of ghost events in the retrieved result. These ghosts are comparable to the spurious multiples as described by Snieder, Wapenaar and Larner (2006) – both appear in the correlation results due to internal multiple scattering. The difference is in the mechanisms that lead to the appearance of the spurious multiples and the ghost events. As Snieder *et al.* (2006) explained, spurious multiples will appear in the case of one-sided illumination (for their example, when in an unbounded medium sources are available only above the receivers). The ghost events that we describe will appear in a dissipative medium even in the case of an isotropic illumination by the sources, which for the case of Fig. 9 means to have subsurface sources distributed along a semicircle. For the unbounded-medium model in Snieder *et al.* (2006), we can link the two mechanisms if we imagine the one-sided illumination as caused by a layer with extremely low quality factor lying below the receivers and absorbing all the energy from sources below it.

In section 'General inhomogeneous subsurface' we identified only one ghost as caused by the losses. The other ghosts, which we expect to see due to internal multiples, are now present also for the lossless situation in Fig. 10(a) because the subsurface source aperture is limited. Using the depiction with the red and green sources in Fig. 9, this would mean, for example, that the red source is available, while the green one is not. As a result, the event along the blue ray will not be compensated. In the general case, it will not be possible to recognize such illumination ghosts as non-physical arrivals unless we know the subsurface velocity model and the source distribution. In practice, though, parts of a non-physical arrival might appear as illumination ghosts and other parts as ghosts due to losses. In this case, the Q-compensation procedure would help to identify the latter parts and consequently the complete non-physical arrival.

Ghosts related to intrinsic losses will appear not only due to internal multiples but due to any scattering. Snieder *et al.* (2008) showed how spurious arrivals, caused by a scatterer in an otherwise homogeneous lossless medium, cancel each other when the illumination from the surrounding sources is isotropic. The cancelling terms are caused on the one hand by cross-correlation of direct and scattered waves and on the other by cross-correlation of two scattered waves. In a lossy medium, these two terms will not cancel mutually as one of them will be weaker. Halliday and Curtis (2009) showed this for surface waves in scattering dissipative media.

In their time-reversal experiment in the presence of dissipation, Tanter *et al.* (1998) assumed the absorbing object (the skull) to be a very thin layer and showed with experimental results that in practice this can be taken to be the case. That the skull acts as a very thin layer means that no internal multiples are generated by it. For this reason the authors have not observed any ghosts after the application of time-reversed imaging. Their compensation factor simply counterbalances the direction-dependent intrinsic losses. The improvement of their result after loss compensation means that such a compensation should improve also our results in Fig. 4(a-c), i.e., the retrieved reflections should become clearer. In our case, though, the Q-compensation resulted also in boosting of the correlation artefacts (resulting from correlation of terms other than only the transmissions, for example correlation of the transmissions with the reflections from the sides of the chamber) and the overall picture did not improve.

We considered the case of a constant-Q intrinsic-loss mechanism, which causes only amplitude changes in the modelled transmission gathers. In practice, intrinsic losses might also cause phase changes in the recorded signals. It needs to be investigated whether the simple amplitude-compensation procedure we proposed would be sufficient to identify loss-related ghosts in this case. If this appears to be insufficient, one should consider a different intrinsic-loss mechanism during the Q-compensation procedure.

In section 'General inhomogeneous subsurface' we showed that in realistic situations it will be difficult to use the Q-compensation procedure also for estimation of the effective Q of the overburden. The best possibilities are provided by the zero-offset traces, assuming that subsurface sources are available in the stationary-phase region for the internal multiples. If one is able to identify all ghosts caused by the internal multiples until a certain depth level by application of the Q-compensation procedure, like in Fig. 7, one could estimate the quality factor of each layer using equation (4) in an iterative scheme. This, of course, assumes that one has information about the subsurface velocity structure. When only a few ghosts can be identified, like in Fig. 10, one has a more difficult task as one would not know unambiguously which layer caused a certain ghost to appear.

If one is only interested in the identification and removal of ghosts due to losses, Ruigrok *et al.* (2009) proposed to use a simpler procedure. A first retrieval result is produced when a correlation is performed with a master trace that contains all arrivals. Then a second retrieval result is produced when the correlation is done with a master trace that contains only the direct arrival. The amplitudes of ghost events in the second result should have increased compared to the amplitudes of the ghost events in the first result. This happens due to the removal of the mutually canceling terms that should eliminate the ghost events (Snieder *et al.* 2008; Vasconcelos and Snieder 2009c). In practice, the difference in the amplitudes might be difficult to see as it might be very small.

The Q-compensation procedure that we proposed for identification of ghosts due to losses needs to be applied to transmission common-source gathers before cross-correlation. This procedure will only work when separate recordings can be made from each of the subsurface sources. In the case of seismic interferometry with white-noise sources in the subsurface, i.e., when the recordings are performed as if the subsurface sources act simultaneously, the ghost events will not be identifiable. In practical situations, though, the noise sources do not always act simultaneously. One can take advantage of this and look at the noise records to identify arrivals from separate subsurface sources. Then one can simulate records from separate subsurface sources, by extracting panels starting around the first arrival and continuing for a few seconds. Draganov (2007) applied this technique to noise records from the Middle East and showed that the interferometry results improve when compared to the interferometry results obtained using the total noise records. When the panels are extracted, each of them should be normalized with the amplitude of its first arrival to compensate for possible unequal damping due to different depth and strength of the subsurface sources and unknown exact time of the first arrival. After that, the panels can be used in the Q-compensation procedure. The Q-compensation and estimation procedure can also be applied to surface waves following a similar preprocessing.

In elastodynamic dissipative media, one will encounter not only loss-related ghosts arising due to P-waves but also ghosts caused by multiple scattering of S-waves and converted waves. Following equation (76) in Wapenaar and Fokkema (2006), one should apply the Q-compensation and estimation procedure to transmission gathers from separate P- and S_k-sources, where $k = 1, 2, 3$.

CONCLUSIONS

Seismic interferometry by cross-correlation assumes a lossless medium. We showed that seismic interferometry by cross-correlation can be used also in a medium with intrinsic losses. We showed with laboratory results from a homogeneous medium that the kinematics of the Green's function are retrieved but that the later arrivals may not be retrieved. We showed that when multiple scattering occurs in the lossy medium, seismic interferometry by cross-correlation gives rise to non-physical events (ghosts) in the retrieved results. These ghosts are a result of internal reflections inside layers lying between the subsurface sources and the receivers. We showed that by applying different Q-compensations to the recorded panels before the cross-correlation, the ghost events can easily be identified, because depending on the strength of the applied compensation they are weakened, they disappear, or they change their polarity. We also demonstrated that the ghosts disappear when the applied Q-compensation corresponds to the value of the effective Q of the overburden above each of the ghost-producing layers. This can be used for effective Q-estimation.

ACKNOWLEDGMENTS

We thank Karel Heller for his assistance in the lab experiments. The research of D.D., the research of R.G. and the lab experiments were financially supported by the Dutch Technology Foundation STW, applied science division of NWO and the technology programme of the Ministry of Economic Affairs (grants VENI.08115 and DAR.5761). The research of E.R. was financially supported by The Netherlands Organisation for Scientific Research NWO (grant Toptalent 2006 AB). We thank the three anonymous reviewers for their very constructive remarks, which helped to improve the manuscript.

REFERENCES

Aki K. and Richards P.G. 2002. *Quantitative Seismology*, 2nd edn. University Science Books.

Campillo M. and Paul A. 2003. Long-range correlations in the diffuse seismic coda. *Science* **299**, 547–549.

Claerbout J.F. 1968. Synthesis of a layered medium from its acoustic transmission response. *Geophysics* **33**, 264–269.

Draganov D. 2007. *Seismic and electromagnetic interferometry: retrieval of the Earth's reflection response using crosscorrelation*. PhD thesis, Delft University of Technology.

Halliday D. and Curtis A. 2009. Seismic interferometry of scattered surface waves in attenuative media. *Geophysical Journal International* (in press).

Hu J.-F. and Su Y.-J. 1999. Estimation of the quality factor in the shallow soil using surface waves. *Acta Seismologica Sinica* **12**, 81–487.

Kjartansson E. 1979. Constant Q-wave propagation and attenuation. *Journal of Geophysical Research* **84**, 4737–4748.

McDonal J.F., Angona F.A., Mills R.L., Sengbush R.L., van Nostrand R.G. and White J.E. 1958. Attenuation of shear and compressional waves in Pierre shale. *Geophysics* **23**, 421–439.

Mittet R. 2007. A simple design procedure for depth extrapolation operators that compensate for absorption and dispersion. *Geophysics* **72**, S105–S112.

Musset A.E. and Khan M.A. 2000. *Looking Into The Earth: An Introduction to Geological Geophysics*. Cambridge University Press.

Priest J.A., Best A.I. and Clayton C.R.I. 2005. Attenuation of seismic waves in methane gas hydrate-bearing sand. *Geophysical Journal International* **164**, 149–159.

Rickett J. and Claerbout J.F. 1996. Passive seismic imaging applied to synthetic data. Stanford Exploration Project, pp. 87–94.

Ruigrok E., Draganov D. and Wapenaar K. 2008. Global-scale seismic interferometry: theory and numerical examples, *Geophysical Prospecting* **56**, 395–417.

Ruigrok E., Wapenaar K., van der Neut J. and Draganov D. 2009. A review of crosscorrelation and multidimensional deconvolution seismic interferometry for passive data. EAGE Workshop on Passive Seismics, Limassol, Cyprus.

Schuster G.T. 2001. Theory of daylight/interferometric imaging: tutorial. 63rd EAGE meeting, Amsterdam, The Netherlands, Extended Abstracts, A–32.

Schuster G.T., Yu J. and Rickett J. 2004. Interferometric/daylight seismic imaging. *Geophysical Journal International* **157**, 838–852.

Schuster G.T. 2009. *Seismic Interferometry*. Cambridge University Press.

Shapiro N.M. and Campillo M. 2004. Emergence of broadband Rayleigh waves from correlations of the ambient seismic noise. *Geophysical Research Letters* **31**, L07614. doi:10.1029/2004GL019491.

Slob E., Draganov D. and Wapenaar K. 2007. Interferometric electromagnetic Green's functions representations using propagation invariants. *Geophysical Journal International* **169**, 60–80.

Snieder R. 2004. Extracting the Green's function from the correlation of coda waves: a derivation based on stationary phase. *Physical Review E* **69**, 046610-1–046610-8.

Snieder R. 2006. Retrieving the Green's function of the diffusion equation from the response to a random forcing. *Physical Review E* **74**, 046620.

Snieder R., Wapenaar K. and Larner K. 2006. Spurious multiples in seismic interferometry of primaries. *Geophysics* **71**, SI111–SI124.

Snieder R. 2007. Extracting the Green's function of attenuating heterogeneous acoustic media from uncorrelated waves. *Journal of the Acoustic Society of America* **121**, 2637–2643.

Snieder R., van Wijk K., Haney M. and Calvert R. 2008. The cancellation of spurious arrivals in Green's function extraction and the generalized optical theorem. *Physical Review E* **78**, 036606.

Tanter M., Thomas J.-L. and Fink M. 1998. Focusing and steering through absorbing and aberrating layers: Application to ultrasonic propagation through the skull. *Journal of the Acoustic Society of America* **103**, 2403–2410.

Tonn R. 1991. The determination of the seismic quality factor *Q* from VSP data: a comparison of different computational methods. *Geophysical Prospecting* **39**, 1–27.

Vasconcelos I. and Snieder R. 2008a. Interferometry by deconvolution, Part 1 - Theory for acoustic waves and numerical examples. *Geophysics* **73**(**3**), S115–S128.

Vasconcelos I. and Snieder R. 2008b. Interferometry by deconvolution, Part 2 - Theory for elastic waves and application to drill-bit seismic imaging, *Geophysics* **73**, S129–S141.

Vasconcelos I. and Snieder R. 2009c. Representation theorems and Green's function retrieval for scattering in acoustic media. *Physical Review E* (in press).

Wapenaar K. and Fokkema J. 2006. Green's functions representations for seismic interferometry. *Geophysics* **71**, SI33–SI46.

Wapenaar K., Slob E. and Snieder R. 2006. Unified Green's function retrieval by cross-correlation. *Physical Review Letters* **97**, 234301-1–234301-4.

Wapenaar K., Draganov D. and Robertsson J.O.A. 2008a. *Seismic Interferometry: History and Present Status*. SEG.

Wapenaar K., Slob E. and Snieder R. 2008b. Seismic and electromagnetic controlled-source interferometry in dissipative media. *Geophysical Prospecting* **56**, 419–434.